

New Insights Into Achievable Spectral Efficiency With Adaptive Free Space Optical Transmissions

Himani Verma, Kamal Singh, and Ranjan K. Mallik, *Fellow, IEEE*

Abstract—Terrestrial free-space optical (FSO) communication systems, while designed to operate on large unlicensed optical bandwidths, are power-constrained due to strict eye safety regulations. The channel fluctuation inherent in terrestrial FSO links also limits the received optical power. Consequently, the available signal-to-noise ratio (SNR) per Hz could become limited; this holds for future long-haul terrestrial systems based on coherent optical communications. An efficient and adaptive transmission mechanism is thus crucial at the optical source. However, a critical assessment of the impact of adaptive transmission in terrestrial FSO systems has received less attention in the literature. This work studies terrestrial FSO communication systems employing adaptive beam transmission while detection receivers operate under shot noise-limited conditions. Specifically, we propose a novel exact closed-form expression for the average spectral efficiency of these FSO systems with transmit beam power adaptation over the gamma-gamma turbulence channel with pointing error. More importantly, we provide a detailed assessment of the impact of turbulence and pointing error impairments on the performance of the aforementioned FSO systems, revealing several novel and counterintuitive insights. In particular, the extensive numerical results help elucidate the intricacies of analyzing these terrestrial FSO systems and clarify a few misconceptions alluded to in recent related literature.

Index Terms—Spectral efficiency, optical beam power adaptation, gamma-gamma turbulence, pointer error, shot noise.

I. INTRODUCTION

Laser-based *free-space optical (FSO) communication* has emerged as an appealing alternative to RF (radio-frequency) and fiber technologies in providing efficient backhaul connectivity in the outdoor wireless networks. The key factors motivating this development are vast unregulated bandwidth, easy installation, inherent security, low-cost transceivers, etc [1]. In fact, interest in the applications of FSO-based wireless technologies has grown rapidly in recent years to design communications for diverse scenarios such as ad hoc wireless networks for tactical and disaster scenarios [1], terrestrial last-mile broadband access [2], deep-space exploration [3], inter-satellite links [4], civil and military applications [5], and the picture is still evolving for 5G and 6G wireless networks.

Most practical FSO communication systems currently in use employ either of the following two detection schemes:

(i) Intensity modulation with direct detection (IM-DD): In intensity-modulated optical systems, the information signal is conveyed by the intensity of the transmitted laser beam, and there is effectively only *one degree of freedom*. At the receiver, the information is detected by direct impingement

of the lightwave signal onto the front-end photodetector. Most commercially deployed FSO systems are based on IM-DD due to their simpler and low-cost transceiver design. However, the IM-DD scheme suffers from poor receiver sensitivity which, in turn, restricts its usage to short-haul terrestrial links [6], [7]. **(ii) Coherent heterodyne detection (HD):** In coherent optical systems, information can be conveyed by simultaneous modulation of the optical carrier's amplitude and phase components, thus having potential for *two degrees of freedom*. Coherent detection basically refers to the addition of a local optical signal (typically of different wavelength and hence 'heterodyne') to the incoming beam prior to photodetection. The coherent HD scheme has better receiver sensitivity which can be traded off with the deployment distance. Additionally, the coherent receiver selects desired channel (in electrical domain) using sharp RF filters and thus offers good selectivity. In contrast, the IM-DD receiver selects a desired optical signal using wideband optical filters and thus suffers severely from poor selectivity. For a detailed review of coherent optical receivers, see [7].

Terrestrial FSO communication systems face two main practical challenges despite their appealing virtues: first, FSO communication is susceptible to the atmospheric turbulence-induced channel fluctuations over a faster time-scale, and to the attenuation effects of scattering and absorption on a much slower time-scale [8]. Second, since FSO communication is essentially *line-of-sight (LOS)* that rely on the highly directional beams and photodetectors, the optical link is prone to pointing errors caused by dynamic wind loads, Tx-Rx motion, thermal expansion, building sway, etc. Both these factors, in unison or individually, are capable of degrading the performance of an FSO communication system drastically [9].

Several statistical models for the small-scale intensity fluctuations are available in the FSO communication literature with a strong basis in realistic terrestrial propagation conditions. We mention a select few important and relevant models as follows: scintillation in weak turbulence is well modeled using log-normal distribution [10], [11], while the scintillation statistic in the weak-to-strong turbulence regimes is best described by gamma-gamma (GG) distribution [11]. Adjacently, the statistical modeling of the pointing error (jitter only) effect in the received irradiance is carried out in [12] while the pointing error case with non-zero boresight is modeled in [13]. More recently, generalized turbulence models are proposed based on Málaga (\mathcal{M}) distribution [14], double-generalized gamma distribution [15], Fisher-Snedecor \mathcal{F} distribution [16], etc.

The terrestrial FSO communication systems are designed to support virtually unlimited and unregulated bandwidth (several GHz in practice) [9]. On the other hand, the emitted optical power is constrained due to stringent eye safety regulations. The available power per hertz can hence become limited

Himani Verma and Kamal Singh are with the Department of Electrical Engineering, Shiv Nadar Institution of Eminence, Delhi NCR, 201314, India (e-mail: hv790@snu.edu.in; kamal.singh@snu.edu.in).

Ranjan K. Mallik is with the Department of Electrical Engineering, Indian Institute of Technology, Delhi, Haus Khas, New Delhi 110016, India (email: rkmallik@ee.iitd.ernet.in).

in practice. Further, the irradiance fluctuations inherent in terrestrial FSO links also degrade the power at the receiver [8], which can be alleviated through adaptive beam transmission. Hence, adaptive FSO communication systems becomes practically important, especially for future high-bandwidth and long-haul terrestrial applications. For example, a naive scheme where the optical transmitter emits power only when the instantaneous channel is good (above a certain threshold), might be reasonable at a low power budget. Despite its practical significance, a critical assessment of adaptive terrestrial FSO communication systems has attracted much less attention in the literature so far, as detailed below.

Several studies exist, that analyze the achievable spectral efficiency (SE) performance of terrestrial FSO systems based on IM-DD and HD detection schemes operating over GG and Log-normal turbulence conditions (see [17], [18], [19], [20], [21], [22] and references cited therein), and recently over generalized turbulence channels (see [23], [24], [25], [26] and references cited therein), etc. However, almost all of these research works have not considered the crucial aspect of beam power adaptation at the optical transmitters for terrestrial FSO links (except for [17], [18], [19]). This is perhaps due to analytical difficulties in solving the optimization problems involved. An infinite series solution for the SE is proposed in [18] for the HD detection based FSO communication system with beam power adaptation over GG turbulence channel, which, however, suggests truncation error related concerns besides the interpretation difficulty. Further, exact and asymptotic SE expressions are derived in [17]-[18], and [19], respectively for the adaptive (beam power) IM-DD-based-FSO system operating in thermal noise-limited conditions over GG turbulence channels. However, in this case, the SE maximization problem is *non-convex* (Remark 1); a fundamental fact which is overlooked in the analyses presented in [17], [18], [19]. Recently, a unified SE expression for the IM-DD and HD schemes under Málaga (\mathcal{M}) distribution (GG distribution is a special case) is developed in [24] but for the ‘no beam power adaptation’ case. It should also be pointed out that the numerical results presented in several related FSO works [17], [20], [21], [23] and [24] lacks clarity on how a wide range of turbulence conditions is realized. Several of the FSO channel parameters are intertwined; for example, varying the FSO link-length alters the turbulence statistics (and path loss) as well as the pointing jitter statistics. Understanding these channel parameters interrelations (and their underlying physics) for the chosen turbulence profiles is crucial, and if neglected, may lead to confusion and flawed insights.

In order to address these research gaps, we will utilize adaptive beam transmission on existing terrestrial FSO communication systems with an emphasis on spectral efficiency improvement, which basically relies on exploiting the temporal channel fluctuations due to turbulence and pointing error impairments. Specifically, this work aims to generate concrete useful insights into the operation of terrestrial FSO communication systems, and provide a baseline SE performance for future adaptive FSO systems with strong practical constraints.

We summarize the principal contributions of this paper as follows.

- We present a novel and unified exact closed-form expression for the average spectral efficiency (ASE) of beam power adaptation-based FSO communication systems with IM-DD and HD detection based receivers subjected to GG turbulence and pointing error. Theorem 1 (resp. Corollary 1) is our main result derived for the turbulent channel with (resp. without) pointing error.
- To present a comprehensive assessment of the fading effects of turbulence and pointing error on the FSO systems performance, the exact solution is further simplified in the asymptotic regimes of optical powers (Theorem 2) providing insights on the ASE losses/gains in these terrestrial links.
- Among the several concrete and counterintuitive insights, we mention the two most important results: i) at high SNRs, the ASE of the optical channel with pointing error improves with turbulence (see Fig. 2), and also that ii) at low SNRs, the ASE improves with turbulence (see Fig. 6). These interesting ASE penalties/improvements are further characterized and justified in greater detail.
- The derived exact closed-form ASE expressions are also validated through extensive Monte Carlo simulations over a wide range of turbulence channel conditions and pointing errors, and for a wide SNR range as well.

The paper is organized as follows. The optical turbulence and pointing error models adopted in this work are described in subsection II-A. The relevant noise sources and the considered FSO receiver models are described in subsections II-B and II-C, respectively. The spectral efficiency theorems are derived in Section III and their extensive numerical analysis is presented in Section IV. Finally, we review our main results and offer some concluding remarks in the Section V.

II. CHANNEL AND SYSTEM MODELS

A. Gamma–Gamma Turbulence with Pointing Error

The (overall) intensity fluctuation, also known as fading in the FSO literature, I of a transmitted laser beam due to atmospheric turbulence and pointing error is modeled as

$$I = I_l I_a I_p \quad (1)$$

where I_l is the path loss component determined by the exponential Beers-Lambert Law for a given link length and weather conditions [27], I_a is the turbulence-induced fluctuation, and I_p is the pointing-error induced fluctuation. In this work, we consider that $I_l = 1$. Next, we describe the statistical models adopted for these independent fading constituents.

Gamma–Gamma Atmospheric Turbulence: The statistics of the intensity fluctuation I_a , covering a wide range of atmospheric turbulence from the weak-to-strong regime, is well modeled using the gamma-gamma (GG) distribution as

$$f_{I_a}(I_a) = \frac{2(ab)^{(a+b)/2}}{\Gamma(a)\Gamma(b)} I_a^{(a+b)/2-1} K_{a-b} \left(2\sqrt{ab}I_a \right); I_a > 0 \quad (2)$$

where a and b are the distribution’s shape parameters [11], $\Gamma(\cdot)$ is the Gamma function [28, Eq. (8.310.1)], and $K_\nu(\cdot)$ is the modified Bessel function of the second kind and order ν [28, Eq. (8.494.1)]. Under the assumption of plane wave optical radiation at the (far away) receiver, the GG distribution

parameters a and b can be directly related to atmospheric conditions as

$$a = 1/\left[\exp(0.49\sigma_R^2/(1+1.11\sigma_R^{12/5})^{7/6})-1\right], \quad (3)$$

$$b = 1/\left[\exp(0.51\sigma_R^2/(1+0.69\sigma_R^{12/5})^{5/6})-1\right], \quad (4)$$

where $\sigma_R^2 = 1.23 C_n^2 k_w^{7/6} L^{11/6}$ denotes the Rytov variance determining the atmospheric turbulence strength, $k_w = 2\pi/\lambda_w$ is the optical wave number, λ_w is the wavelength, L is the propagation distance, and C_n^2 is the index of refraction structure parameter [11].

Pointing Error: Pointing error is a mispointing of the laser beam w.r.t. the optical receiver that arises from i) boresight and ii) jitter: boresight is the *fixed* displacement between the received beam centroid and the detection receiver center, whereas jitter is the *random* temporal displacement originating due to building sway, wind motion, Tx/Rx vibrations, etc.

In this work, we consider a terrestrial FSO link between *fixed platforms* where it is reasonable that the boresight problem can be made negligible by either careful system deployment or using a fast-tracking transmitter whereas the random jitter issue persists [8]. Upon propagating a distance L , the laser beam of waist w_L is incident on the receiving photodetector with an aperture radius r_A [29]. The received optical beam attenuation due to turbulence-induced beam spread with pointing error (the misalignment is described by radial displacement r in the receiver plane between the centers of the beam footprint and the detector aperture) is given by $I_p(r; L) \approx A_0 \exp(-2r^2/w_{\text{Leq}}^2)$ where $w_{\text{Leq}}^2 = w_L^2 \sqrt{\pi} \operatorname{erf}(v)/(2v \exp(-v^2))$ is the (squared) equivalent beam width with $v = \sqrt{\pi} r_A / \sqrt{2} w_L$, and the fraction of the collected power at $r = 0$ [30] is

$$A_0 = [\operatorname{erf}(v)]^2, \quad (5)$$

where $\operatorname{erf}(\cdot)$ denotes the standard error function [28, Eq. (8.250.1)]. Note that $0 \leq A_0 \leq 1$. For a coherent collimated beam, the beam radius w_L is related to the beam waist w_0 at the exit aperture of the optical transmitter by $w_L = w_0(1 + \epsilon(\lambda_w L/\pi w_0^2))^{1/2}$ where $\epsilon = (1 + 2w_0^2/\rho_0^2(L))$ is the global coherence parameter and $\rho_0(L) = (1.46C_n^2 k_w^2 L)^{-3/5}$ is the coherence length of a plane wave propagating in turbulence [31]. Farid and Hranilovic [30] derived the PDF of the irradiance component I_p under the i.i.d. zero-mean Gaussian distribution assumptions for both the horizontal and vertical sways at the receiver (i.e., zero boresight and identical jitters) and is given by

$$f_{I_p}(I_p) = \frac{\xi^2}{A_0} I_p^{\xi^2-1}; \quad 0 \leq I_p \leq A_0 \quad (6)$$

where the parameter $\xi \triangleq w_{\text{Leq}}/2\sigma_e$ is the ratio of the received equivalent beam waist w_{Leq} and the standard deviation of the pointing error displacement (jitter) at the detection receiver. It is important to keep in mind that the probability model (6) for pointing error is reasonable when $w_L/r_A \gg 1$ and further that the effects of ξ and A_0 parameters are independent [30]. More recently, a new pointing jitter model is proposed in [32], which is shown to be more accurate for some particular FSO systems and channel settings. Since Farid's model offers a little more generality, we have considered it in our work.

Composite Fading Distribution: Given the distributions in (2) and (6) of the independent constituents I_a and I_p , the PDF of the instantaneous composite irradiance $I = I_a I_p$ is developed to [17, Eq. (8)]

$$f_I(I) = \frac{ab\xi^2}{A_0\Gamma(a)\Gamma(b)} G_{1,3}^{3,0} \left(\frac{abI}{A_0} \middle| \begin{matrix} \xi^2 \\ \xi^2 - 1, a - 1, b - 1 \end{matrix} \right). \quad (7)$$

B. Noise Sources in FSO Wireless Systems

Two fundamental sources of noise interfere in the process of photodetection: i) the shot noise due to photodetection itself [33], and ii) the thermal noise in the receiver circuitry. The shot noise is due to the information optical radiation and the ambient light incident on the receiver lens, and its power grows linearly with the total incident optical power. Both the ambient shot noise and thermal noise are *signal-independent* since they are statistically independent of the information optical signal [34].

The IM-DD photodetector output is composed of desirable photocurrent component mapped one-to-one to the intensity of the incoming (information) optical signal, signal-dependent shot noise current, ambient shot noise current, and thermal noise current. The IM-DD receiver operation mode is determined from the relative strengths of these noise components as follows.

- For an IM-DD receiver operating in intense ambient light conditions and/or strong thermal noise conditions, it is reasonable that the corrupting noise is signal-independent. It typically holds for indoor IM-DD infrared *diffuse or non-LOS* links [35].
- For the IM-DD based FSO systems with large received optical information-signal powers, it is reasonable to expect the corrupting noise to be signal-dependent [36]. It is valid for short-haul and/or medium-haul laser-based IM-DD *LOS directed* links with reasonable transmit powers [35].

In a coherent HD receiver, an optical local oscillator (OLO) signal is *mixed* to the received signal prior to photodetection. This introduces an *OLO-dependent* shot noise in addition to the signal shot noise, the ambient noise, and the thermal noise. By ensuring a large OLO optical power, the OLO shot noise component can be made dominant compared to other noise components; this is in fact considered to be the *de facto* mode of operation of an (ideal) coherent HD receiver [7], [34], [37].

A short note on the statistical properties of the shot noise: when the number of received photons per symbol period is insignificant (e.g., in inter-satellite and ground-satellite optical links), a Poisson model is adequate; otherwise, a Gaussian model suffices [38]. The Gaussian approximation is adequate for most terrestrial application systems; for a rigorous proof of the Gaussian distribution of the high-intensity shot noise, refer [38], [39].

C. Receiver Models

Let $x_{\text{IMDD}} \in \mathbb{R}^+$ and $x_{\text{HD}} \in \mathbb{C}$ denote the transmitted signals for the IM-DD and coherent HD systems respectively. We remind the reader that the baseband (information) signal in a coherent HD scheme represents a complex optical field, whereas the baseband signal in an IM-DD scheme represents optical intensity. In both schemes, the transmitted beam power is constrained by a fixed average power constraint denoted by: $\mathbb{E}[x_{\text{IMDD}}] \leq P_{\text{avg}}$ and $\mathbb{E}[|x_{\text{HD}}|^2] \leq P_{\text{avg}}$. Adhering to this understanding, the received signal models for the two detection systems are developed next.

1) *Signal-Dependent IM-DD Receiver System*: The baseband signal in an IM-DD receiver is described by

$$y_{\text{IMDD}} = I x_{\text{IMDD}} + \sqrt{I x_{\text{IMDD}}} n_{\text{SD}} + n_{\text{SI}} \quad (8)$$

where y_{IMDD} is the received signal, I is the intensity fluctuation (see (7)), $n_{\text{SI}} \sim \mathcal{N}(0, \sigma_{\text{SI}}^2)$ is the signal-independent noise (combined ‘ambient and thermal noise’) modeled as additive white Gaussian noise (AWGN), and the $\sqrt{I x_{\text{IMDD}}} n_{\text{SD}} \sim \mathcal{N}(0, I x_{\text{IMDD}} \sigma^2)$ is the signal-dependent AWGN [36].

Remark 1. *In the signal-independent noise-limited IM-DD operation, $n_{\text{SI}} \gg \sqrt{I x_{\text{IMDD}}} n_{\text{SD}}$ with high probability. Hence, the received SNR ($:= I^2 x_{\text{IMDD}}^2 / \sigma_{\text{SI}}^2$) varies as the ‘square’ of the received optical power. In [17], [18], [19], the average SE maximization problem for the signal-independent noise-limited IM-DD channel is formulated as $\mathbb{E}[\ln(1 + I^2 P^2(I))]$ where $P^2(I) := x_{\text{IMDD}}^2$ under the constraint $\mathbb{E}[P(I)] = P_{\text{avg}}$; this is a non-convex optimization, and more seriously, the above SE formulation ignored the non-negativity constraint on I (see [40] for details).*

In this work, we consider the signal-dependent noise-limited IM-DD receiver; thus, the noise power is dominated by $I x_{\text{IMDD}} \sigma^2$. Hence, conditioned on I , the instantaneous received SNR is

$$\gamma_{\text{IMDD}} = I x_{\text{IMDD}} / \sigma^2. \quad (9)$$

Notice from (9) that the SNR varies *linearly* with the incident optical power at the considered IM-DD receiver.

2) *Coherent Heterodyne Detection Receiver System*: The complex baseband signal in a coherent HD receiver is given by

$$y_{\text{HD}} = h x_{\text{HD}} + w_{\text{OLO}} + w_{\text{OTHER}} \quad (10)$$

where $y_{\text{HD}} \in \mathbb{C}$ represents its output, $h \in \mathbb{C}$ the fluctuation in the received optical field, $w_{\text{OLO}} \sim \mathcal{CN}(0, \sigma_{\text{OLO}}^2)$ the OLO shot noise, and w_{OTHER} the total AWGN from all the sources other than the OLO [10, Ch. 3]. The OLO shot noise is the only dominant noise of consequence. Hence, conditioned on h or more appropriately on $I := |h|^2$, the instantaneous received SNR is

$$\gamma_{\text{HD}} = I |x_{\text{HD}}|^2 / \sigma_{\text{OLO}}^2. \quad (11)$$

III. ACHIEVABLE SPECTRAL EFFICIENCY WITH ADAPTIVE OPTICAL BEAM TRANSMISSION

The transmitted signal x_{IMDD} , being optical intensity, is non-negative, while the x_{HD} scheme suffers from no such limitation and in fact can support two degrees of freedom. Consequently, the well-known Shannon limit on spectral efficiency of the AWGN channel is applicable in the HD scheme but not in the IM-DD system (see [40]). Conditioned on the received SNRs in (9) and (11), the SE of the optical channels (in nats/s/Hz) based on IM-DD and HD schemes satisfy

$$S_{\text{IMDD}}(I) \geq \frac{1}{2} \ln \left(1 + \frac{\gamma_E}{2\pi} \frac{I x_{\text{IMDD}}}{\sigma^2} \right), \quad (12)$$

$$S_{\text{HD}}(I) = \ln \left(1 + \frac{I |x_{\text{HD}}|^2}{\sigma_{\text{OLO}}^2} \right). \quad (13)$$

In (12), the constant γ_E is the Euler’s constant. The lower bound (12) on the achievable SE of the signal-dependent IM-DD channel is deduced from a well-known result in [40, Theorem 7]

derived for the AWGN IM-DD channel under average-power constraint. Specifically, the lower bound converges to the actual SE for high received optical powers [40, Proposition 8]. The bound is in fact an accurate estimate of the actual SE since an IM-DD channel with high received optical power is considered. Based on (12) and (13), a unified SE expression for a given channel state $\lambda := I$ can be given for both the FSO systems as follows.

$$S(\lambda) := \frac{1}{k} \ln \left(1 + \frac{\lambda P_k(\lambda)}{N_k} \right) \quad (14)$$

where $k = 1$ for the HD based scheme with $N_1 = \sigma_{\text{OLO}}^2$, $P_1(\lambda) := |x_{\text{HD}}|^2$, and $k = 2$ for the IM-DD based scheme with $N_2 = \sigma^2 / (\gamma_E / 2\pi)$, $P_2(\lambda) := x_{\text{IMDD}}$. The power constraint mentioned earlier for both these schemes gets translated to $\mathbb{E}[P_k(\lambda)] \leq P_{\text{avg}}$.

The **average spectral efficiency** (ASE) in nats/s/Hz is given by

$$\bar{S} = \max_{P_k} \frac{1}{k} \mathbb{E} \left[\ln \left(1 + \frac{\lambda P_k(\lambda)}{N_k} \right) \right] \quad (15)$$

where the maximization is over the set of all feasible transmit laser beam adaptation schemes satisfying $\mathbb{E}[P_k(\lambda)] \leq P_{\text{avg}}$. The optimal beam power adaptation P_k^* which maximizes (15) is

$$\frac{P_k^*(\lambda)}{N_k} = \left(\frac{1}{\mu_k} - \frac{1}{\lambda} \right)^+ \quad (16)$$

with μ_k chosen so that the optical power constraint

$$\mathbb{E} \left[\left(\frac{1}{\mu_k} - \frac{1}{\lambda} \right)^+ \right] = \text{SNR}_k \quad (17)$$

is satisfied. Note that in (17), $\text{SNR}_k := P_{\text{avg}} / N_k$ is the average transmit power normalized by the average noise power. Notice that the parameter μ_k also acts as a channel cutoff and hence the ASE problem in (15) gets simplified to

$$\bar{S} = \frac{1}{k} \int_{\mu_k}^{\infty} \ln \left(\frac{\lambda}{\mu_k} \right) f_{\lambda}(\lambda) d\lambda. \quad (18)$$

To compute \bar{S} , we bifurcate the integral in (18) into three parts as follows:

$$\bar{S} = \frac{1}{k} \left[\underbrace{\int_0^{\infty} \ln(\lambda) f_{\lambda}(\lambda) d\lambda}_{=I_1} - \underbrace{\int_0^{\mu_k} \ln(\lambda) f_{\lambda}(\lambda) d\lambda}_{=I_2} - \underbrace{\int_{\mu_k}^{\infty} \ln(\mu_k) f_{\lambda}(\lambda) d\lambda}_{=I_3} \right]. \quad (19)$$

In the evaluation of the integrals I_1 , I_2 and I_3 , we will repeatedly make use of an integral identity involving the Meijer-G function [28, Eq. (9.301)], as noted below [41].

$$\int x^{j-1} G_{p,q}^{m,n} \left(x \left| \begin{matrix} a_1, \dots, a_p \\ b_1, \dots, b_q \end{matrix} \right. \right) dx = G_{p+1,q+1}^{m,n+1} \left(x \left| \begin{matrix} 1, j+a_1, \dots, j+a_n, j+a_{n+1}, \dots, j+a_p \\ j+b_1, \dots, j+b_m, 0, j+b_{m+1}, \dots, j+b_q \end{matrix} \right. \right). \quad (20)$$

A. Exact ASE With and Without Pointing Errors

Theorem 1. For the GG turbulence channel with pointing error and perfect channel state information (CSI) at both ends, the exact ASE is given by

$$\bar{S} = \frac{1}{k} \left[\ln \left(\frac{A_0}{ab} \right) + \psi(a) + \psi(b) - \ln(\mu_k) - \left(\frac{1}{\xi^2} \right) + \frac{\xi^2}{\Gamma(a)\Gamma(b)} G_{3,5}^{3,2} \left(\frac{ab}{A_0} \mu_k \left| \begin{matrix} 1, 1, \xi^2 + 1 \\ \xi^2, a, b, 0, 0 \end{matrix} \right. \right) \right] \quad (21)$$

where $\psi(\cdot)$ is the Euler's digamma function, and μ_k is determined from $\int_{\mu_k}^{\infty} (1/\mu_k - 1/\lambda) f_\lambda(\lambda) d\lambda = \text{SNR}_k$.

Proof: The unified ASE expression (from (19)) is

$$\bar{S} = (I_1 - I_2 - I_3)/k. \quad (22)$$

Evaluation of Integral I_1 : The integral I_1 can be viewed as

$$I_1 = \mathbb{E} [\ln \lambda]. \quad (23)$$

We reformulate (23) by taking expectation on the identity $\frac{d}{dt} \lambda^t = \lambda^t \ln(\lambda)$ and thereupon evaluating at $t = 0$ such that

$$\mathbb{E} [\lambda^t \ln(\lambda)] \Big|_{t=0} = \frac{d}{dt} (\mathbb{E} [\lambda^t]) \Big|_{t=0}$$

$$\text{and hence } I_1 = \frac{d}{dt} \left(\int_0^{\infty} \lambda^t f_\lambda(\lambda) d\lambda \right) \Big|_{t=0}. \quad (24)$$

The t -th moment in the RHS of (24) is computed as

$$\int_0^{\infty} \lambda^t f_\lambda(\lambda) d\lambda = \frac{ab\xi^2}{A_0\Gamma(a)\Gamma(b)} \int_0^{\infty} \lambda^t G_{1,3}^{3,0} \left(\frac{ab\lambda}{A_0} \left| \begin{matrix} \xi^2 \\ \xi^2 - 1, a - 1, b - 1 \end{matrix} \right. \right) d\lambda. \quad (25)$$

Applying (20) in (25) along with the substitutions that

$$\lim_{x \rightarrow 0} G_{2,4}^{3,1} \left(x \left| \begin{matrix} 1, \xi^2 + t + 1 \\ \xi^2 + t, a + t, b + t, 0 \end{matrix} \right. \right) = 0, \quad \text{and} \\ \lim_{x \rightarrow \infty} G_{2,4}^{3,1} \left(x \left| \begin{matrix} 1, \xi^2 + t + 1 \\ \xi^2 + t, a + t, b + t, 0 \end{matrix} \right. \right) = \frac{\Gamma(a+t)\Gamma(b+t)}{\xi^2 + t},$$

we have

$$I_1 = \frac{\xi^2}{\Gamma(a)\Gamma(b)} \frac{d}{dt} \left(\left(\frac{A_0}{ab} \right)^t \frac{\Gamma(a+t)\Gamma(b+t)}{\xi^2 + t} \right) \Big|_{t=0}. \quad (26)$$

Upon differentiation w.r.t. t and then evaluating the attained expression for $t = 0$, we obtain the final I_1 expression as

$$I_1 = \ln \left(\frac{A_0}{ab} \right) + \psi(a) + \psi(b) - \left(\frac{1}{\xi^2} \right). \quad (27)$$

In the above, we have used $d(\ln \Gamma(x))/dx = \psi(x)$.

Evaluation of Integral I_2 : The integral part I_2 is now evaluated as

$$I_2 = \int_0^{\mu_k} \ln(\lambda) f_\lambda(\lambda) d\lambda \\ = \frac{ab\xi^2}{A_0\Gamma(a)\Gamma(b)} \int_0^{\mu_k} \ln(\lambda) G_{1,3}^{3,0} \left(\frac{ab\lambda}{A_0} \left| \begin{matrix} \xi^2 \\ \xi^2 - 1, a - 1, b - 1 \end{matrix} \right. \right) d\lambda.$$

We apply the integration-by-parts technique treating $\ln(\cdot)$ as the first function and the Meijer-G function as the second to get

$$I_2 = \left[G_{2,4}^{3,1} \left(\frac{ab\lambda}{A_0} \left| \begin{matrix} 1, \xi^2 + 1 \\ \xi^2, a, b, 0 \end{matrix} \right. \right) \times \ln(\lambda) - G_{3,5}^{3,2} \left(\frac{ab\lambda}{A_0} \left| \begin{matrix} 1, 1, \xi^2 + 1 \\ \xi^2, a, b, 0, 0 \end{matrix} \right. \right) \right] \Big|_{\lambda=0}^{\lambda=\mu_k} \times \frac{\xi^2}{\Gamma(a)\Gamma(b)}. \quad (28)$$

With the Meijer-G function limits

$$\lim_{x \rightarrow 0} G_{2,4}^{3,1} \left(x \left| \begin{matrix} 1, \xi^2 + 1 \\ \xi^2, a, b, 0 \end{matrix} \right. \right) \times \ln(x) = 0, \quad \text{and}$$

$$\lim_{x \rightarrow 0} G_{3,5}^{3,2} \left(x \left| \begin{matrix} 1, 1, \xi^2 + 1 \\ \xi^2, a, b, 0, 0 \end{matrix} \right. \right) = 0,$$

the final I_2 expression is given by

$$I_2 = \left[G_{2,4}^{3,1} \left(\frac{ab}{A_0} \mu_k \left| \begin{matrix} 1, \xi^2 + 1 \\ \xi^2, a, b, 0 \end{matrix} \right. \right) \times \ln(\mu_k) - G_{3,5}^{3,2} \left(\frac{ab}{A_0} \mu_k \left| \begin{matrix} 1, 1, \xi^2 + 1 \\ \xi^2, a, b, 0, 0 \end{matrix} \right. \right) \right] \frac{\xi^2}{\Gamma(a)\Gamma(b)}. \quad (29)$$

Evaluation of Integral I_3 : The I_3 component is given as

$$I_3 = \ln(\mu_k) \int_{\mu_k}^{\infty} f_\lambda(\lambda) d\lambda, \quad (30)$$

where the integral is computed as

$$\int_{\mu_k}^{\infty} f_\lambda(\lambda) d\lambda \\ = 1 - \frac{ab\xi^2}{A_0\Gamma(a)\Gamma(b)} \int_0^{\mu_k} G_{1,3}^{3,0} \left(\frac{ab\lambda}{A_0} \left| \begin{matrix} \xi^2 \\ \xi^2 - 1, a - 1, b - 1 \end{matrix} \right. \right) d\lambda \\ = 1 - \frac{\xi^2}{\Gamma(a)\Gamma(b)} G_{2,4}^{3,1} \left(\frac{ab}{A_0} \mu_k \left| \begin{matrix} 1, \xi^2 + 1 \\ \xi^2, a, b, 0 \end{matrix} \right. \right). \quad (31)$$

The last equality is obtained by applying the identity in (20) along with the substitution that

$$\lim_{x \rightarrow 0} G_{2,4}^{3,1} \left(x \left| \begin{matrix} 1, \xi^2 + 1 \\ \xi^2, a, b, 0 \end{matrix} \right. \right) = 0.$$

Substituting these I_1, I_2 and I_3 expressions back into (22) and consequent simplification gives the final closed-form expression of the ASE in Theorem 1. ■

The ASE with dynamic beam power adaptation over the GG turbulence channel (but without pointing error) is a useful baseline for comparison as follows.

Corollary 1. For the GG turbulence channel 'without pointing error' and perfect CSI at both ends, the exact ASE is given by

$$\bar{S} = \frac{1}{k} \left[\ln \left(\frac{1}{ab} \right) + \psi(a) + \psi(b) - \ln(\mu_k) + \frac{1}{\Gamma(a)\Gamma(b)} G_{2,4}^{2,2} \left(ab\mu_k \left| \begin{matrix} 1, 1 \\ a, b, 0, 0 \end{matrix} \right. \right) \right] \quad (32)$$

where μ_k is solved from $\int_{\mu_k}^{\infty} (1/\mu_k - 1/\lambda) f_\lambda(\lambda) d\lambda = \text{SNR}_k$.

Proof: For the $A_0 \rightarrow 1$ and $\xi^2 \rightarrow \infty$ choices, the fading distribution tends to the (pure) GG distribution. Allowing these limiting values of ξ and A_0 in (21) along with the identity [28, Eq. (9.31.1)] completes the proof of the theorem. ■

To the best of the authors' knowledge, the proposed exact ASE solutions, Theorems 1 and Corollary 1, for the GG turbulence channels with and without pointing error are new.

B. Immediate Insights

The proposed ASE formula is interesting in obtaining quantitative as well as qualitative insights as follows.

- At high SNRs, contribution from the Meijer-G based term vanishes while $\mu_k \rightarrow 1/\text{SNR}_k$. Keeping this in mind, and now comparing the ASE of channels with and without pointing error, the ASE loss due to pointing error can be easily quantified in terms of A_0 and ξ^2 parameters.
- Likewise, the ASE loss due to both turbulence and pointing error at high SNR when compared with no channel impairments (pure AWGN) can also be quantified and analyzed.
- In a fixed terrestrial FSO link, variation in turbulence can lead to change in the pointing error behavior. In such a scenario, the derived closed-form ASE expression also allows an accurate analysis of the impact of these interlinked channel parameters.

More in-depth and broader expositions into adaptive transmission benefit and impact of channel impairments will be presented in Section IV by allowing wide range variations of the channel turbulence and/or the pointing error, and SNRs as well.

C. Low-SNR and High-SNR Asymptotic Expressions

The asymptotic expansions of the derived exact ASE expressions provide clear insights into (how) the key parameters of the fading phenomenon (both GG fading and pointing error) that determine the performance of these FSO schemes.

To this end, we first derive μ_k - SNR_k dependence from the average power constraint in the low and high SNR regimes.

Lemma 1. *The threshold value μ_k associated with the optimal beam power adaptation as described in (16) for the transmitted laser beam satisfies*

- 1) At high SNR: $\mu_k \approx \frac{1}{\text{SNR}_k}$,
- 2) At low SNR: $\mu_k \approx \frac{A_0}{4ab} \ln^2 \left(\frac{1}{\text{SNR}_k} \right)$.

Proof: Part 1): Substituting (7) into the average optical power constraint (17), we have

$$\frac{\mu_k \text{SNR}_k}{A} = \int_{\mu_k}^{\infty} \left(1 - \frac{\mu_k}{\lambda}\right) G_{1,3}^{3,0} \left(\frac{ab\lambda}{A_0} \middle| \xi^2 - 1, a - 1, b - 1 \right) d\lambda,$$

where $A = ab\xi^2/(A_0\Gamma(a)\Gamma(b))$. Applying the identity in (20) to the power constraint equation gives

$$\begin{aligned} \frac{\mu_k \text{SNR}_k}{A} &= \frac{1}{A} - \frac{A_0}{ab} G_{2,4}^{3,1} \left(\frac{ab}{A_0} \mu_k \middle| 1, \xi^2 + 1 \right) \\ &\quad + \mu_k G_{2,4}^{3,1} \left(\frac{ab}{A_0} \mu_k \middle| \xi^2 - 1, a - 1, b - 1, 0 \right). \end{aligned} \quad (33)$$

We deduce from the power constraint (17) that μ_k bears a strictly monotone relation with SNR_k . Precisely, μ_k decreases as SNR_k increases and vice versa. We particularly note that the contributions from both the Meijer-G functions based terms in (33) for small inputs (due to high SNRs) are vanishingly small and hence

$$\lim_{\mu_k \rightarrow 0} \mu_k \text{SNR}_k = 1.$$

This completes the proof of 1).

Part 2): In this part, we seek to obtain an explicit expression for the μ_k - SNR_k dependence at low SNRs. Since the cutoff μ_k

increases as SNR_k decreases, the optical transmitter allocates power *only* for very high channel gains at low SNRs. First, we approximate the distribution function of the channel gain $f_\lambda(\lambda)$ in (7) using the low-order series expansion of the Meijer's G function for large input arguments provided below:

$$G_{1,3}^{3,0} \left(z \middle| \xi^2 - 1, a - 1, b - 1 \right) \approx e^{-2\sqrt{z}} \sqrt{\pi} z^{\frac{1}{4}(-7+2a+2b)}. \quad (34)$$

Only the largest term in the series expansion is shown in (34) which is then substituted on the LHS of the average power constraint (17) to yield

$$\text{SNR}_k \approx K [B_1(\bar{\mu}_k)/\bar{\mu}_k - B_2(\bar{\mu}_k)] \quad (35)$$

where $K = (\sqrt{\pi} ab \xi^2)/(A_0 \Gamma(a) \Gamma(b))$ is a positive constant independent of the threshold value, and

$$B_1(\bar{\mu}_k) = \Gamma(n + 1, 2\sqrt{\bar{\mu}_k})/2^n, \quad (36)$$

$$B_2(\bar{\mu}_k) = 4\Gamma(n - 1, 2\sqrt{\bar{\mu}_k})/2^n, \quad (37)$$

where, in turn, $\bar{\mu}_k = ab\mu_k/A_0$ is the scaled threshold value, $n = a + b - \frac{5}{2}$, and the $\Gamma(\cdot, \cdot)$ is the upper incomplete Gamma function whose power series expansion at large input is given below [28]:

$$\Gamma(s, t) \approx t^s e^{-t} \left(\frac{1}{t} + \frac{s-1}{t^2} + o\left(\frac{1}{t}\right)^3 \right). \quad (38)$$

By considering only the first two largest terms in (38), (35) gets simplified to

$$\text{SNR}_k \approx K \left(\frac{ab}{A_0} \mu_k \right)^{\left(\frac{a+b}{2} - \frac{11}{4}\right)} e^{-2\sqrt{\frac{ab}{A_0} \mu_k}}. \quad (39)$$

Taking the logarithm on both sides of (39) and considering only the most significant term by the relative order of magnitude in the right-hand side above, we obtain

$$\ln(\text{SNR}_k) \approx -2\sqrt{ab\mu_k/A_0}. \quad (40)$$

Solving (40) for μ_k , we finally arrive at

$$\mu_k \approx \frac{A_0}{4ab} \ln^2 \left(\frac{1}{\text{SNR}_k} \right). \quad (41)$$

This completes the proof of 2). ■

Theorem 2. *For the GG turbulence channel with pointing error, the asymptotic ASE at low and high SNR are given by*

$$\bar{S}_{low} \approx \frac{1}{k} \left[\frac{A_0}{4ab} \text{SNR}_k \ln^2 \left(\frac{1}{\text{SNR}_k} \right) \right], \quad \text{and} \quad (42)$$

$$\bar{S}_{high} \approx \frac{1}{k} \left[\ln \text{SNR}_k + \ln \left(\frac{A_0}{ab} \right) + \psi(a) + \psi(b) - \left(\frac{1}{\xi^2} \right) \right] \quad (43)$$

where the subscripts 'low' and 'high' stand for the low-SNR (asymptotically 0) and high-SNR (asymptotically ∞) regimes respectively.

Proof: Part 1): At high SNR, the threshold follows $\mu_k \approx \text{SNR}_k^{-1}$ (from lemma 1) while the Meijer's G function becomes insignificant for small input argument (asymptotically 0) as

$$\lim_{z \rightarrow 0} G_{3,5}^{3,2} \left(z \middle| 1, 1, \xi^2 + 1 \right) = 0. \quad (44)$$

With these substitutions in Theorem 1, (43) is proved.

Part 2): The low-order series expansion of the Meijer-G function in (21) for large input argument z (asymptotically ∞) is

$$G_{3,5}^{3,2} \left(z \left| \begin{matrix} 1, 1, \xi^2 + 1 \\ \xi^2, a, b, 0, 0 \end{matrix} \right. \right) \approx e^{-2\sqrt{z}} \sqrt{\pi} z^{\frac{1}{4}(-7+2a+2b)} + \frac{\Gamma(a)\Gamma(b)}{\xi^2} \left(\ln(z) + \frac{1}{\xi^2} - \psi(a) - \psi(b) \right). \quad (45)$$

Substituting the above series expansion in (21), we observe

$$\bar{S} \approx \frac{K}{k(ab/A_0)} \left(\frac{ab}{A_0} \mu_k \right)^{\left(\frac{a+b}{2} - \frac{7}{4} \right)} e^{-2\sqrt{\frac{ab}{A_0} \mu_k}}. \quad (46)$$

Comparing (46) with (39) derived in connection with the lemma 1, we find that

$$\bar{S} \approx \frac{\mu_k \text{SNR}_k}{k}. \quad (47)$$

Finally, substituting μ_k from (41) in (47) completes the proof of the low SNR ASE expansion (42) in Theorem 2. ■

A few interesting observations from the derived theorems are as follows.

- By applying $A_0 \rightarrow 1$ and $\xi^2 \rightarrow \infty$, the asymptotic ASEs of the GG turbulence channel ‘without pointing error’ at low and high SNR are computed as

$$\bar{S}_{low} \approx \frac{1}{k} \left[\frac{1}{4ab} \text{SNR}_k \ln^2 \left(\frac{1}{\text{SNR}_k} \right) \right], \quad \text{and} \quad (48)$$

$$\bar{S}_{high} \approx \frac{1}{k} \left[\ln \text{SNR}_k + \ln \left(\frac{1}{ab} \right) + \psi(a) + \psi(b) \right]. \quad (49)$$

- By comparing (43) and (49), a measure of the ASE degradation due to pointing errors at high SNRs can be found as

$$\frac{1}{k} \left[\frac{1}{\xi^2} - \ln A_0 \right]. \quad (50)$$

- For the GG turbulence channel, the presence of pointing errors decreases the ASE at low SNRs by A_0 times.

The derived asymptotic results in (42), (43), (48) and (49) are useful for a comprehensive assessment of the impact of variations of turbulence and pointing error statistics over a wide range.

IV. NUMERICAL RESULTS AND DISCUSSION

In this section, we highlight the analytical utilities of the derived ASE formulae with the help of extensive numerical results. Several earlier studies on the closely related topics [17], [20], [21], [23] and [24], suggest both directly and indirectly that a wide range of atmospheric turbulence conditions are attainable by varying the FSO link length. Unfortunately, link length variation also impacts large-scale path loss. The situation is further complicated because the laser beam waist expands with propagation distance, affecting the pointing error distribution parameters ξ and A_0 . However, none of these earlier studies have accounted for these intricacies and ignored these inter-relations. Understanding these interrelated channel characteristics is crucial as our research focuses on accurately identifying and analyzing the impact of wide turbulence and pointing error variations on the ASE performance of terrestrial FSO systems.

To ensure a fair comparison and provide meaningful insights, the FSO Tx-Rx system parameters are maintained constant (optical wavelength, Tx. beam-waist, Rx. aperture, etc.). Equally

TABLE I
FSO SYSTEM AND CHANNEL SETTINGS

Parameter	Symbol	Value
Optical wavelength	λ_w	1550 nm
Beam waist (at Tx.)	w_0	1.2 cm
FSO channel length	L	1800 m
Rx. Aperature radius	r_A	1.5 cm
Tx./Rx. optics efficiency	–	100% (assumed)
Path loss factor	–	Unity (assumed)
<i>Gamma-Gamma (GG) fading Parameters</i>		
Turbulence strength	Rytov variance σ_R^2	GG distribution parameters
Weak	0.8	$a = 4.7424, b = 3.0133$
Moderate	2	$a = 3.9929, b = 1.7018$
Strong	6	$a = 4.8184, b = 1.1896$
<i>GG fading with pointing error Parameters</i> <i>Jitter std. deviation $\sigma_e = 0.1$ m (fixed)</i>		
Turbulence strength	Rytov variance σ_R^2	Pointing Error distribution parameters
Weak	0.8	$\xi = 0.4790, A_0 = 0.0490$
Moderate	2	$\xi = 0.6302, A_0 = 0.0283$
Strong	6	$\xi = 1.0269, A_0 = 0.0107$

important, a horizontal terrestrial FSO link of fixed length is considered, keeping the path loss factor *unchanged*. Table I shows the adopted Tx-Rx settings typical in many practical terrestrial FSO communication systems [8], [9]. To achieve a wide turbulence range in the terrestrial FSO link without affecting the path loss, we recall that the atmospheric turbulence strength is dictated by $\sigma_R^2 = 1.23 C_n^2 k_w^{7/6} L^{11/6}$ which underscores its dependence on the index of refraction structure parameter C_n^2 as remarked below.

Remark 2. For a near-ground horizontal propagation path, the parameter C_n^2 remains unchanged and varies with height above ground [8, Section 12.2]; strong turbulence near ground level whereas weak turbulence at high altitudes [42, Ch. 2].

A few more important considerations before proceeding with the numerical results are as follows.

- As discussed in the introduction, a key fundamental difference between the two FSO wireless systems, namely IM-DD and HD-based communication systems, is that they have very different amount of noise levels [7]. For concreteness, we assume that the noise power levels (per Hz) in both detection receivers are the same, i.e., $N_1 = N_2 = N_0$, say.
- Notice that $\text{SNR} := P_{\text{avg}}/N_0$ is the average transmit SNR in all the derived ASE formulae (with subscript k now suppressed from the SNR symbol as the noise levels are assumed the same) and that the horizontal axis in Figures 1–8 is the transmit SNR in log scale, not the received SNR. This ensures fair comparison and accurate analysis mentioned earlier. If required, the average received SNR can be computed by scaling the transmit SNR by the mean channel gain $\mathbb{E}[\lambda]$.
- Note that in all the figures to follow, we plot ASE values (bits/sec/Hz is the unit of measurement) by multiplying the derived ASE formulae by $1/(\ln 2)$.

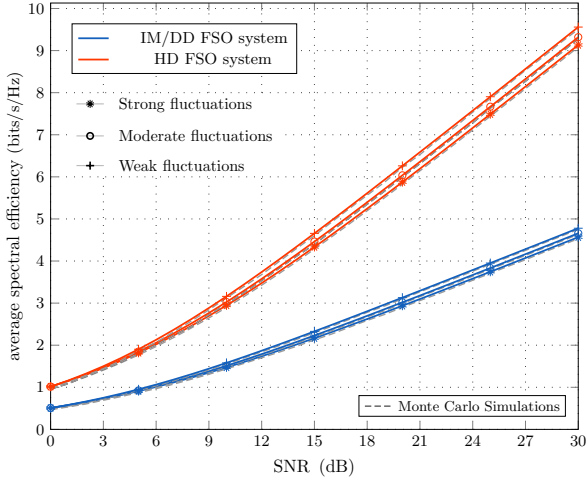


Fig. 1. Average spectral efficiency of the GG turbulence channel without pointing error under HD and IM-DD detection schemes. The average received SNR is the same as the transmit SNR since the mean channel gain $\mathbb{E}[\lambda] = 1$.

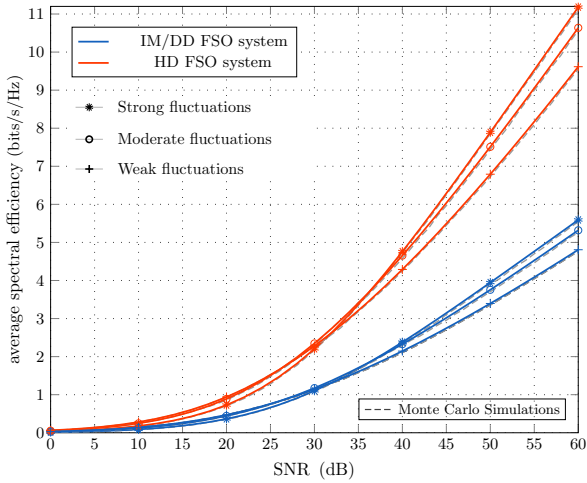


Fig. 2. Average spectral efficiency of the GG turbulence channel with pointing jitter under HD and IM-DD detection schemes. The received SNR is less than the transmit SNR by $\mathbb{E}[\lambda] = -22.6$ (dB) for strong turbulence in Table I.

Exact ASE behavior: Using Theorem 1, the exact ASE of the HD and IM-DD based optical channels under GG turbulence without and with pointing errors are computed and plotted in Figures 1 and 2 respectively. These values are in excellent agreement with the values obtained by Monte Carlo simulations for varying turbulence levels and pointing jitters over a wide SNR range displayed in these figures.

Discussion: Two interesting observations can be drawn from Figures 1 and 2:

- A sharp decline in the channel spectral efficiency at high SNRs is noticeable in the presence of pointing error. A quick and intuitive justification for this behavior is that the received SNR is degraded by the factor $A_0 \xi^2 / (1 + \xi^2)$ due to pointing error.
- Fig. 1 shows the decay of the spectral efficiency with turbulence at high SNRs for both the detection schemes. The higher the turbulence strength, the greater the loss in spectral efficiency; this is expected and can be easily explained by noticing that the probability distribution of the channel gains (especially low gains) is severed with increasing turbulence

conditions (refer Fig. 7). The opposite is true in the presence of pointing error as shown in Fig. 2: for a given pointing error, spectral efficiency improves at high SNR for stronger turbulence conditions which is very surprising. The explanation to this unexpected ASE behavior is a bit involved. Hence, we next analyze the asymptotic behavior in the high SNR regime.

ASE behavior at High SNRs: The asymptotic ASE behavior at high SNRs described by (43) in Theorem 2 suggests a comparison with the channel ASE without any turbulence and pointing error, which is the well-known AWGN channel SE given by $\ln \text{SNR}$ (at high SNRs). This difference, overall being negative-valued, can be viewed as *spectral efficiency loss/penalty at high SNRs* due to the combined effect of GG fading and pointing jitter, i.e.,

$$\bar{S}_{\text{penalty}} \triangleq \ln \left(\frac{A_0}{ab} \right) + \psi(a) + \psi(b) - \left(\frac{1}{\xi^2} \right). \quad (51)$$

Discussion: Fig. 3 plots the spectral efficiency penalty (51) (red curve) as a function of the strength of the atmospheric turbulence. Recall that we have considered a fixed-length horizontal FSO link with a collimated laser beam at the transmitter with the beam waist of $w_0 = 1.2$ cm (see Table I). The beam footprint at the receiver (after propagating over 1.8 km) is expanded due to atmospheric turbulence conditions. This enlarged beam size has two effects:

- the fraction of the power collected at the fixed-aperture receiver is reduced (i.e., A_0 decreases), and
- the impact of the pointing jitter effect at the receiver is weakened (i.e., ξ increases).

The beam enlargement due to greater turbulence yields an increase in spectral efficiency at high SNRs because the reduction in the pointing jitter effect more than compensates for the loss in collected power at the receiver, as shown in Fig. 3 for $\sigma_R^2 \leq 6$. Eventually, for very strong turbulence conditions, the pointing jitter effect becomes negligible while the loss in collected power continues leading to loss in spectral efficiency, as shown in Fig. 3 for $\sigma_R^2 > 6$. We also notice from Fig. 3 that this penalty (at high SNRs) for different turbulence conditions can vary by a large amount (approximately -13 to -8.5 bits/s/Hz).

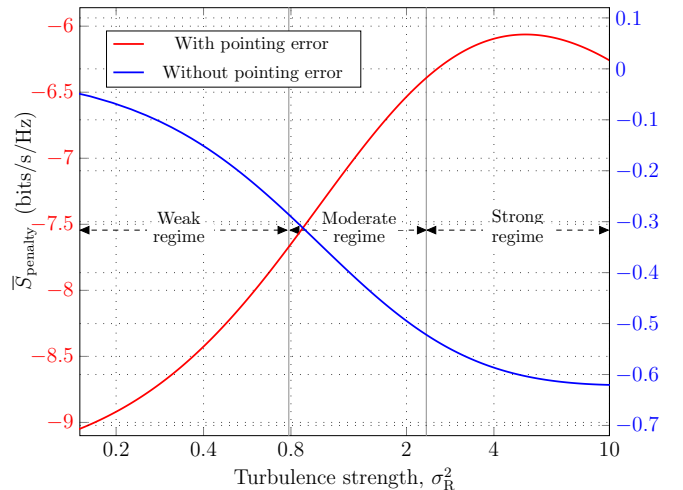


Fig. 3. The loss in Spectral efficiency at high SNRs as a function of turbulence strength for the GG channel with and without pointing jitter under HD detection scheme.

In the GG fading without pointing error, on the other hand, the penalty at high SNRs is described by (see (49))

$$\bar{S}_{\text{penalty}} = \psi(a) + \psi(b) - \ln(ab) \quad (52)$$

and is plotted as blue curve in Fig. 3. Here, the penalty is monotonically increasing with turbulence and the extent of the penalty is relatively small (approximately -0.9 to -0.1 bits/s/Hz) in comparison with the penalty associated with both fading and pointing error.

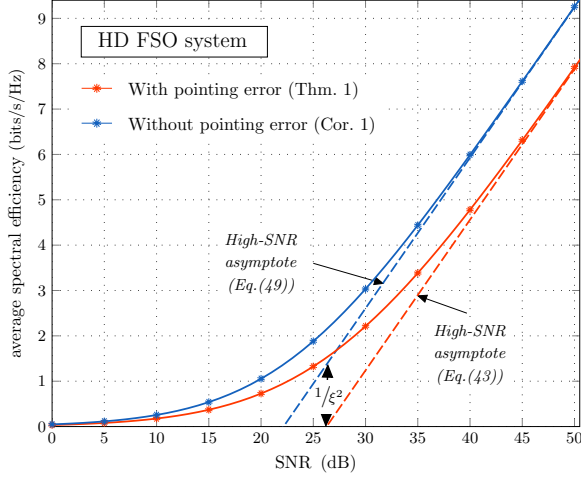


Fig. 4. Spectral efficiency for ‘Strong’ GG turbulence channels under HD scheme (see 3rd row in Table I). $A_0 = 0.0107$ for both exact and asymptotic results in both GG channels with and without pointing error.

In almost all the existing mentioned related works, the parameter A_0 is neglected for optical fading without pointing error which is inaccurate; A_0 can in fact be small for a fading channel without pointing jitter. For an accurate comparison, it is important to consider A_0 in both with and without pointing error cases, as illustrated in Fig. 4.

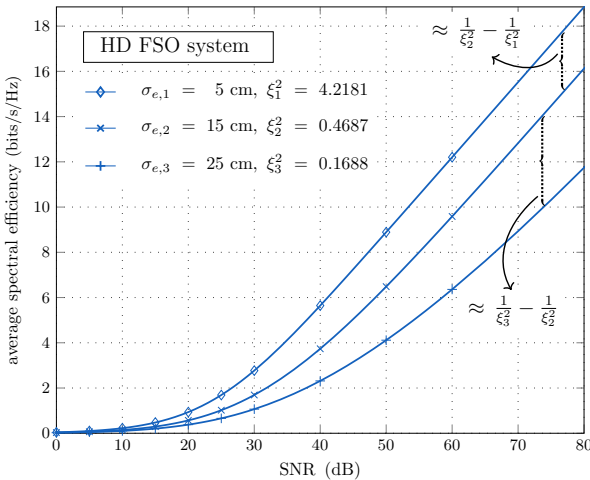


Fig. 5. Spectral efficiency of ‘Strong’ GG turbulence channel under HD scheme for varying levels of pointing jitter’s std. dev. σ_e (or ξ^2 equivalently).

In the ‘fixed-length’ optical channel with a fixed FSO system setting as we have considered, it is also possible to estimate the impact of increasing pointing jitter. Recall that σ_e is the pointing jitter’s standard deviation. The loss in spectral efficiency

(in nats/s/Hz) at high SNRs due to an increase in jitter (only) can be easily deduced from (43) and is given by

$$\bar{S}_{\text{loss}, \Delta\xi} \approx \frac{1}{k} \left[\frac{1}{\xi_{\text{new}}^2} - \frac{1}{\xi_{\text{old}}^2} \right] = \frac{4(\sigma_{e,\text{new}}^2 - \sigma_{e,\text{old}}^2)}{kw_{L_{\text{eq}}}^2} \quad (53)$$

where $w_{L_{\text{eq}}}$ is the (fixed) received equivalent beam waist. This is numerically illustrated in Fig. 5.

ASE behavior at Low SNRs: As motivated in the introduction, it is practically interesting to understand the spectral efficiency of terrestrial FSO links operating at low SNRs. The power control aspect of the transmitted laser beam becomes important at low-power budgets which necessitates exploiting the channel fading efficiently.

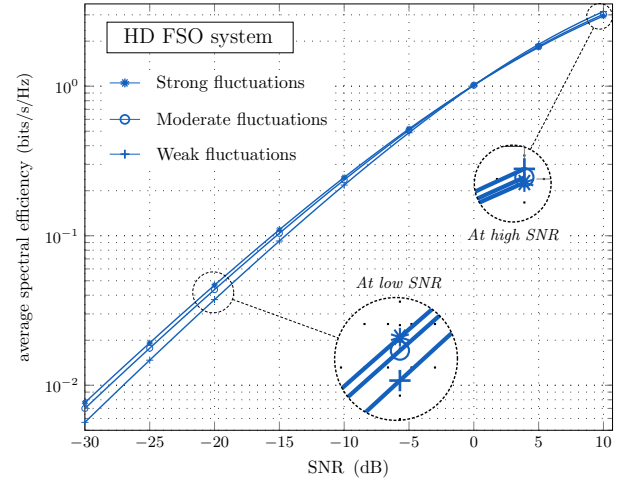


Fig. 6. Spectral efficiency at low SNRs for the GG turbulence channel without pointing jitter under HD detection scheme (see Table I for turbulence settings).

Discussion: Fig. 6 plots the exact spectral efficiency for the GG fading channel without pointing error under the HD detection scheme at low SNRs. Somewhat surprisingly, the low-SNR spectral efficiency shows improvement with increasing turbulence, which can also be confirmed from (48); specifically, increasing GG turbulence conditions, say from turbulence profile (a_i, b_i) to the new (a_j, b_j) , yield

$$\text{ASE improvement factor} \approx \frac{a_j b_j}{a_i b_i} \text{ at low SNR.} \quad (54)$$

This improvement in the spectral efficiency is completely justified by noticing that the distribution of the higher channel gains improves with turbulence as shown in Fig. 7, which is exploited by the transmitter operating at low SNR (with full CSI) with beam power adaptation in an optimized manner. More precisely, the improved tail probability with turbulence suggests that the optical transmitter observes higher channel gains more often under higher turbulence conditions, and hence, in turn, allocates more beam power for better channel gains and no power is wasted for weaker channel states, resulting in an overall improvement in spectral efficiency at low SNRs as illustrated in Fig. 6.

On the other hand, the impact of turbulence on the spectral efficiency of the optical channel ‘with’ pointing error at low SNRs becomes more involved. As shown in Fig. 8, the spectral efficiency at low SNRs first shows a very slight improvement in

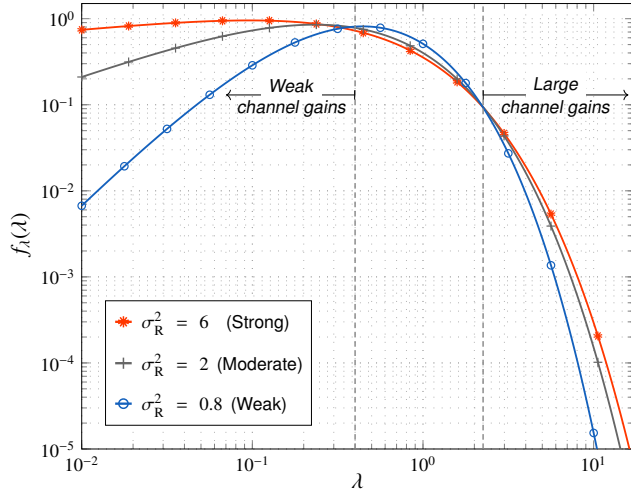


Fig. 7. The PDF of the GG fading gain for the settings described in Table I. Notice the larger probabilities for the higher gains with increasing turbulence.

the weak turbulence regime, but then subsequently deteriorates over the moderate-to-strong turbulence regime.

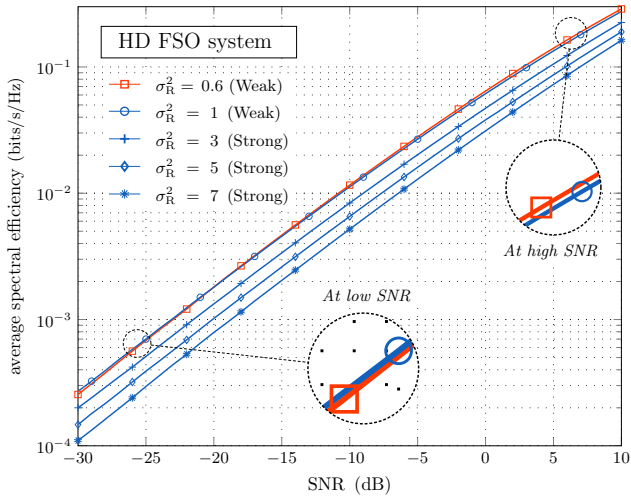


Fig. 8. Spectral efficiency results in the low SNR regime for Gamma-Gamma turbulence channel 'with' pointing jitter under HD detection scheme.

This peculiar characteristic can be explained using the asymptotic low-SNR spectral efficiency result (42) in Theorem 2: the overall effect of both atmospheric turbulence and pointing error on the optical channel spectral efficiency at very low SNR (but fixed) is summarily captured in the term $A_0/(4ab)$ which is rearranged as

$$\text{turbulence scaled factor} \triangleq A_0 \times \frac{1}{4ab}. \quad (55)$$

Fig. 9 plots the variation of the scaled factor (55) (red curve) with turbulence, along with the factor $1/4ab$ (blue curve) which is valid for the pure optical turbulence (see (48)). On comparing the two curves, we find that the parameter A_0 (which indicates the fraction of collected power) degrades with turbulence: first slowly in the weak fluctuation regime and then rapidly in strong fluctuation conditions while the factor $1/4ab$ increases. To get some intuition about the variation of A_0 with turbulence, the reader can take a look at the A_0 entries in the Table I described for some typical values of weak, moderate and strong turbulence

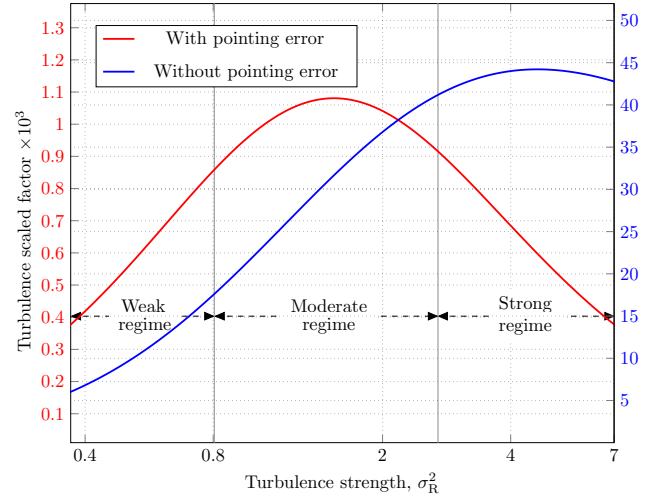


Fig. 9. Variation of the turbulence scaled factor for the GG turbulence channel under HD detection scheme.

conditions. Overall, except for weak fluctuations, the channel spectral efficiency at low SNRs with both fading and pointing error typically degrades with turbulence strength over a wide range of moderate-to-strong conditions.

V. CONCLUSION

In this work, we have analyzed the average spectral efficiency of terrestrial FSO communication systems over gamma-gamma turbulence channels with beam power adaptation incorporated at the optical transmitter side. The analysis also detailed the negative impact on the performance due to pointing errors impairments present in typical FSO links.

The proposed exact solutions are explicit: the impact of the fading and pointing error parameters are accurately identified, especially in the extreme SNR regimes. Most notably, we have shown an interesting interplay between the pointing error parameters A_0 and ξ^2 with the variation in turbulence conditions: as the turbulence increases (from weak conditions), there is a rapid improvement in achievable spectral efficiency in the high SNR regime because the reduction in the pointing jitter effect more than compensates for the loss in received power. On the other hand, for a fading channel without pointing error, the average spectral efficiency expectedly degrades with turbulence at high SNRs.

We have shown that at low SNRs, the average spectral efficiency in the optical channel can be improved with turbulence. This happens due to two reasons: i) the distribution of the higher fading gains improves with turbulence, and ii) the transmitter exploits higher gains (or peaks) more efficiently through beam power control. However, with pointing error, the distribution of higher gains degrades severely with turbulence leading to spectral efficiency loss at low SNRs. From a practical standpoint, terrestrial FSO communication at low SNRs can be very appealing for two reasons: firstly, the presence of the limited optical power per hertz constraint especially for future high-bandwidth and long-haul applications, and secondly, the fact that communication in a power-limited regime is more energy-efficient. In this context, characterization of spectral efficiency of a coherent FSO system at low SNRs derived in this work becomes significant.

REFERENCES

- [1] S. Arnon, J. Barry, G. Karagiannidis, R. Schober, and M. Uysal, *Advanced Optical Wireless Communication Systems*. Cambridge, U.K.: Cambridge Univ. Press, 2012.
- [2] Q. Liu, C. Qiao, G. Mitchell, and S. Stanton, "Optical wireless communication networks for first- and last-mile broadband access," *IEEE/OSA J. Opt. Netw.*, vol. 4, no. 12, p. 807–828, 2005.
- [3] D. Cornwell, "Laser communication from the Moon at 622Mb/s."
- [4] F. Heine, H. Kämpfner, R. Czichy, R. Meyer, and M. Lutzer, "Optical inter-satellite communication operational," in *Proc. IEEE Military Communications Conference (MILCOM)*, 2010, pp. 1583–1587.
- [5] H. Haan and M. Tausendfreund, "Free-space optical data transmission for military and civil applications: A company report on technical solutions and market investigation," in *2013 15th International Conference on Transparent Optical Networks (ICTON)*. IEEE, 2013, pp. 1–4.
- [6] D. J. Heatley, D. R. Wisely, I. Neild, and P. Cochrane, "Optical wireless: The story so far," *IEEE Commun. Mag.*, vol. 36, no. 12, pp. 72–74, 1998.
- [7] J. R. Barry and E. A. Lee, "Performance of coherent optical receivers," *Proceedings of the IEEE*, vol. 78, no. 8, pp. 1369–1394, 1990.
- [8] L. C. Andrews and R. L. Phillips, *Laser Beam Propagation Through Random Media: Second Edition*. SPIE Press, Bellingham, Wash., 2005.
- [9] S. Bloom, E. Korevaar, J. Schuster, and H. Willebrand, "Understanding the performance of free-space optics," *Journal of Optical Networking*, vol. 2, no. 6, pp. 178–200, 2003.
- [10] S. Karp, R. M. Gagliardi, S. E. Moran, and L. B. Stotts, *Optical Channels: Fibers, Clouds, Water, and the Atmosphere*. Springer Science & Business Media, 2013.
- [11] M. Al-Habash, L. C. Andrews, and R. L. Phillips, "Mathematical model for the irradiance probability density function of a laser beam propagating through turbulent media," *Optical Engineering*, vol. 40, no. 8, pp. 1554–1562, 2001.
- [12] A. A. Farid and S. Hranilovic, "Outage capacity optimization for free-space optical links with pointing errors," *Journal of Lightwave Technology*, vol. 25, no. 7, pp. 1702–1710, 2007.
- [13] F. Yang, J. Cheng, and T. A. Tsiftsis, "Free-space optical communication with nonzero boresight pointing errors," *IEEE Transactions on Communications*, vol. 62, no. 2, pp. 713–725, 2014.
- [14] A. Jurado-Navas, J. M. Garrido-Balsells, J. F. Paris, A. Puerta-Notario, and J. Awrejcewicz, "A unifying statistical model for atmospheric optical scintillation," in *Numerical Simulations of Physical and Engineering Processes*. Intech Rijeka, Croatia, 2011, vol. 181, no. 8, pp. 181–205.
- [15] M. A. Kashani, M. Uysal, and M. Kavehrad, "A novel statistical channel model for turbulence-induced fading in free-space optical systems," *Journal of Lightwave Technology*, vol. 33, no. 11, pp. 2303–2312, 2015.
- [16] K. P. Peppas, G. C. Alexandropoulos, E. D. Xenos, and A. Maras, "The fisher–snedecor \mathcal{F} -distribution model for turbulence-induced fading in free-space optical systems," *Journal of Lightwave Technology*, vol. 38, no. 6, pp. 1286–1295, 2020.
- [17] W. Gappmair, "Further results on the capacity of free-space optical channels in turbulent atmosphere," *IET Communications*, vol. 5, no. 9, pp. 1262–1267, 2011.
- [18] M. Z. Hassan, M. J. Hossain, and J. Cheng, "Ergodic capacity comparison of optical wireless communications using adaptive transmissions," *Opt. Express*, vol. 21, no. 17, pp. 20 346–20 362, Aug 2013.
- [19] F. Benkhelifa, Z. Rezki, and M.-S. Alouini, "Low snr capacity of FSO links over gamma-gamma atmospheric turbulence channels," *IEEE Communications Letters*, vol. 17, no. 6, pp. 1264–1267, 2013.
- [20] I. S. Ansari, F. Yilmaz, and M.-S. Alouini, "Performance analysis of FSO links over unified gamma-gamma turbulence channels," in *IEEE 81st Vehicular Technology Conference (VTC Spring)*, 2015, pp. 1–5.
- [21] I. E. Lee, Z. Ghassemlooy, W. P. Ng, M.-A. Khalighi, and S.-K. Liaw, "Effects of aperture averaging and beam width on a partially coherent Gaussian beam over free-space optical links with turbulence and pointing errors," *Applied Optics*, vol. 55, no. 1, pp. 1–9, 2016.
- [22] H. E. Nistazakis, E. A. Karagianni, A. D. Tsigopoulos, M. E. Fafalios, and G. S. Tombras, "Average capacity of optical wireless communication systems over atmospheric turbulence channels," *Journal of Lightwave Technology*, vol. 27, no. 8, pp. 974–979, 2009.
- [23] H. AlQuwaiee, I. S. Ansari, and M.-S. Alouini, "On the performance of free-space optical communication systems over double generalized gamma channel," *IEEE Journal on Selected Areas in Communications*, vol. 33, no. 9, pp. 1829–1840, 2015.
- [24] I. S. Ansari, M.-S. Alouini, and J. Cheng, "Ergodic capacity analysis of free-space optical links with nonzero boresight pointing errors," *IEEE Trans. Wirel. Commun.*, vol. 14, no. 8, pp. 4248–4264, 2015.
- [25] O. S. Badarneh, R. Derbas, F. S. Almeahadi, F. El Bouanani, and S. Muhaidat, "Performance analysis of fso communications over \mathcal{F} turbulence channels with pointing errors," *IEEE Communications Letters*, vol. 25, no. 3, pp. 926–930, 2021.
- [26] Y. M. Shishter, F. H. Ali, and R. C. Young, "Performance analysis of fso communications over a generalized turbulence fading channel with pointing error," *Transactions on Emerging Telecommunications Technologies*, vol. 35, no. 2, p. e4935, 2024.
- [27] H. Weichel, *Laser Beam Propagation in the Atmosphere*. SPIE Optical Engineering Press, Bellingham, 1990.
- [28] I. S. Gradshteyn and I. M. Ryzhik, *Table of Integrals, Series, and Products*, 7th ed. San Diego, CA: Academic Press, Inc., 2007.
- [29] B. E. Saleh and M. C. Teich, *Fundamentals of Photonics*. John Wiley & Sons, Ltd, 2019.
- [30] A. A. Farid and S. Hranilovic, "Outage capacity optimization for free-space optical links with pointing errors," *Journal of Lightwave Technology*, vol. 25, no. 7, pp. 1702–1710, 2007.
- [31] J. C. Ricklin and F. M. Davidson, "Atmospheric turbulence effects on a partially coherent Gaussian beam: implications for free-space laser communication," *Journal of the Optical Society of America A, Optics, Image Science, and Vision*, vol. 19, no. 9, pp. 1794–1802, Sept. 2002.
- [32] M. Miao, X.-y. Chen, R. Yin, and J. Yuan, "New results for the pointing errors model in two asymptotic cases," *IEEE Photonics Journal*, vol. 15, no. 3, pp. 1–7, 2023.
- [33] B. Oliver, "Thermal and quantum noise," *Proceedings of the IEEE*, vol. 53, no. 5, pp. 436–454, 1965.
- [34] G. P. Agrawal, *Fiber-Optic Communication Systems*, 3rd ed. New York: Wiley, 2002.
- [35] J. Kahn and J. Barry, "Wireless infrared communications," *Proceedings of the IEEE*, vol. 85, no. 2, pp. 265–298, 1997.
- [36] S. M. Moser, "Capacity results of an optical intensity channel with input-dependent Gaussian noise," *IEEE Transactions on Information Theory*, vol. 58, no. 1, pp. 207–223, 2012.
- [37] K. Kikuchi, "Fundamentals of coherent optical fiber communications," *Journal of Lightwave Technology*, vol. 34, no. 1, pp. 157–179, 2015.
- [38] A. Chaaban, Z. Rezki, and M.-S. Alouini, "On the capacity of intensity-modulation direct-detection Gaussian optical wireless communication channels: A tutorial," *IEEE Communications Surveys & Tutorials*, vol. 24, no. 1, pp. 455–491, 2021.
- [39] E. A. Lee and D. G. Messerschmitt, *Digital Communication*. Springer Science & Business Media, 2012.
- [40] A. Lapidoth, S. M. Moser, and M. A. Wigger, "On the capacity of free-space optical intensity channels," *IEEE Transactions on Information Theory*, vol. 55, no. 10, pp. 4449–4461, 2009.
- [41] Wolfram Research, Inc., "The Wolfram Functions website." Available: <https://functions.wolfram.com/07.34.21.0002.01>. [Accessed on 16-03-2025].
- [42] R. R. Beldand, *Propagation through Atmospheric Optical Turbulence. The Infrared and Electro-Optical Systems Handbook*, F. G. Smith, ed. (SPIE Optical Engineering Press, Bellingham, Washington), 1993, vol. 2.